Pyrolysis of Furan: Ab Initio Quantum Chemical and Kinetic Modeling Studies

Karina Sendt, George B. Bacskay,*,† and John C. Mackie*,‡

School of Chemistry, University of Sydney, NSW 2006, Australia

Received: October 5, 1999; In Final Form: December 14, 1999

The kinetics of pyrolysis of furan have been investigated theoretically by ab initio quantum chemical techniques and by detailed chemical kinetic modeling of previously reported experimental results. [Organ, P. P.; Mackie, J. C. *J. Chem. Soc., Faraday Trans.* **1991**, *87*, 815.] The kinetic model, containing rate constants derived from the ab initio calculations, can satisfactorily model the species profiles that had been obtained in shock tube experiments at three initial concentrations of furan. The thermochemistry and rate parameters of a number of key reactions have been obtained by ab initio calculations carried out at CASSCF, CASPT2, and G2-(MP2) levels of theory. The calculations suggest that two parallel processes, initiated by 1,2-H transfers that result in the formation of cyclic carbene intermediates and lead to the decomposition products CO + propyne and C_2H_2 + ketene (as major and minor channels, respectively), are the dominant pathways and enable the quantitative modeling of the kinetics of furan disappearance and the formation of the major products. Direct ring scission in furan, either on a singlet or triplet surface, is found to be much too energetic to contribute to any appreciable degree. No evidence was found for significant participation of a third channel producing HCO + C_3H_3. H atoms and C_3H_3 radicals arise essentially by CH fission of propyne. Hydrogen abstraction from furan by methyl radicals is, however, significant and represents the principal source of methane in the products.

Introduction

Thermal decomposition reactions of furan have been studied extensively partly because of the important role that furan and its derivatives play in the combustion of coals and biomass[1] and also because furan is an interesting model compound on which to study vibrational relaxation, incubation, and unimolecular decomposition.[2]

There have been five previous studies of the kinetics of pyrolysis of furan.[2−6] Grela et al.[3] investigated the very low-pressure pyrolysis (VLPP) of furan over the temperature range 1050−1270 K. Only the major products CO and C_3H_4 (propyne/allene) were detected by mass spectrometry, and from an extrapolation of their VLPP data they obtained the value of $k_\infty = 10^{15.6} \exp[-308 \text{ kJ mol}^{-1}/(RT)] \text{ s}^{-1}$ for the rate constant for disappearance of furan. Lifshitz et al.[4] used single pulse shock tube (SPST) methods to study the pyrolysis kinetics of furan dilute in argon at total pressures of about 3 atm over the temperature range 1050−1460 K. From product analyses they concluded that the decomposition was a two-channel process in which one channel produced CO and propyne while the other formed acetylene and ketene. For the overall rate constant for disappearance of furan, Lifshitz et al.[4] obtained the value of $k_{\text{overall}} = 10^{15.43\pm0.45} \exp[-328 \pm 8 \text{ kJ mol}^{-1}/(RT)] \text{ s}^{-1}$ at 3 atm pressure. This value is about a factor of 10 lower than that obtained by Grela et al. Although they identified several decomposition products, Lifshitz et al.[4] were unable to detect ketene in their products. Organ and Mackie[5] studied furan pyrolysis kinetics both by time-resolved infrared absorption spectrometry and by SPST techniques over the temperature range 1100−1700 K at pressures of about 20 atm. They obtained the value $k_{\text{overall}} = 10^{15.3\pm0.3} \exp[-326 \pm 8 \text{ kJ mol}^{-1}/(\text{RT})] \text{ s}^{-1}$, in good agreement with the earlier value of Lifshitz et al.[4] They detected the major products CO, C_3H_4 (propyne/allene), and C_2H_2. Ketene was also detected in the products using FTIR spectroscopy. They postulated that two major decomposition channels led to CO + C_3H_4 and to C_2H_2 + CH_2CO, respectively. They also suggested the possibility of a minor third channel to HCO + C_3H_3 from which the propargyl radicals and H atoms from decomposition of HCO could produce benzene and other hydrocarbons observed in the products.

On the basis of the experimental Arrhenius parameters, all three groups[3−5] assumed that the initial and rate-determining process in furan pyrolysis was CO scission to an open-chain biradical. The good agreement between the Lifshitz et al.[4] kinetics at 3 atm and that of Organ and Mackie[5] at 20 atm gives strong support to the notion that the decomposition of furan is taking place at the high-pressure limit at ∼3 atm and above. In addition, Organ and Mackie[5] used group additivity methods[7] to estimate the enthalpy of formation of the open-chain carbene (triplet) to be approximately 297 kJ mol^{-1} at 300 K or about 332 kJ mol^{-1} in energy above furan, in good agreement with the experimental activation energy, thereby giving further support for the postulate of initiation by CO scission.

A further study of furan pyrolysis kinetics was carried out by Bruinsma et al.[6] in a flow reactor at pressures of ∼0.01 atm and over the limited temperature range 960−1085 K, which partially overlaps the temperatures studied by Lifshitz et al.[4] Although Bruinsma et al.[6] reported very low Arrhenius parameters ($A = 10^{12.9}$ s^{-1} and $E_a = 275$ kJ mol^{-1}), their overall rate constant is in good agreement with that of Lifshitz et al.[4] Finally, a very recent shock tube study of furan pyrolysis has been reported using laser-schlieren densitometry and time-of-flight mass spectrometry conducted at low pressures.[2] The focus of this last investigation was principally to study vibrational

* To whom correspondence should be sent.
† E-mail: bacskay@chem.usyd.edu.au.
‡ E-mail: j.mackie@chem.usyd.edu.au.

10.1021/jp993537b CCC: $19.00
Published on Web 02/11/2000

relaxation and falloff in the decomposition rate, and Fulle et al.[2] accepted the values of Lifshitz et al.[4] and Organ and Mackie[5] for k_∞ for furan disappearance. Fulle et al.[2] supported the postulate of a two-channel decomposition of furan and considered that a third channel to HCO + C_3H_3 could be discounted on thermochemical grounds.

Thus, experiment supports a value of $k_\infty = 10^{15.4\pm0.4}$ exp[-325 ± 10 kJ mol^{-1}/(RT)] s^{-1} for disappearance of furan in the range 1000−1700 K. However, there has been no independent theoretical testing of the assumption that the decomposition is actually initiated by CO fission to an open-chain biradical. Recently, we have been investigating theoretically the initiation of pyrolysis in the analogous heterocycle, pyrrole, by means of ab initio quantum calculations. We found that the reaction of lowest activation energy in pyrrole decomposition is to HCN + propyne, which is initiated via a ring hydrogen shift to form a cyclic carbene with an intact NH bond.[8,9] The theoretically derived initiation rate constant for pyrrole was shown in modeling studies to give good agreement with experimental pyrolysis data.[9] It is therefore instructive to apply ab initio techniques to investigate whether an analogous initiation actually takes place in pyrolysis of furan.

Despite the wealth of quantum chemical studies of properties of furan, we are aware of only two studies of the reactions of furan. First, a study of the photorearrangement of acylcyclopropenes to furans was carried out by Wilsey et al.[10] describing various mechanisms by which furan is formed from excited states of acylcyclopropene. Second, a study of the unimolecular decomposition channels of furan was carried out by Liu et al.[11] using density functional (B3LYP) techniques to compute the geometries and the QCISD(T) method to obtain energies. Although this study reported the energetics of several decomposition pathways, no rate parameters were calculated and thus no comparison with experimental (kinetic modeling) studies was made, nor an investigation of the accepted decomposition mechanism. Thus, there is a need for a comprehensive quantum chemical study in conjunction with kinetic modeling in order to obtain rate parameters for the decomposition reactions and to elucidate the important pathways in the thermal decomposition of furan. Further, since these reactions contain interesting chemical species, some of which may not be detected or properly described using purely single-reference-based techniques, such as density functional or quadratic CI methods, it is important to carefully review the work reported thus far.

The accepted decomposition mechanism, where furan undergoes ring opening via CO bond scission, involves the formation of a carbene species with a considerable potential for π delocalization. This intermediate may have a carbene-like structure (i.e., a substituted methylene) or a biradical structure in which the unpaired electrons are not localized on the same atom. In this work, the triplet biradical was found to be the ground state, but contrary to expectations, the lowest singlet state was found to be a biradical structure in which the two unpaired electrons are singlet-coupled, requiring two-configurational SCF treatment (at minimum) to properly describe the wave function. The carbene-like structure, in which the orbitals are doubly occupied, is therefore an excited singlet state. Other unimolecular decomposition mechanisms also involve carbenes as intermediates, with the possibility of biradical resonance structures for some of these, resulting in a rich and interesting chemistry.

Finally, secondary decomposition reactions of furan have not previously been studied theoretically. Analogous reactions, such as the abstraction of hydrogen from ethylene by methyl radical,[12] would tend to suggest that for a molecule with large CH bond fission energies such as furan, abstraction reactions would not be important. However, owing to the constraint of remaining a ring compound, the transition states for hydrogen abstraction from furan by methyl are considerably more floppy than the ethylene analogues and could result in these pathways being more important than would otherwise be expected.

Theoretical and Computational Methods

The potential energy surfaces (PES) of furan and related compounds were studied by using ab initio quantum chemical methods to obtain geometries, energies, and vibrational frequencies of reactants, intermediates, transition states, and products. For all species, the complete active space SCF (CASSCF) method[13,14] was used to obtain geometries and vibrational frequencies, with Dunning's cc-pVDZ basis set.[15,16] The energies were computed at these geometries at the CASPT2[17,18] level of theory using Dunning's cc-pVTZ basis sets.[16] In this work, a CASSCF calculation with nel active electrons in an active space of nao active orbitals will be denoted CASSCF(nel/nao). In the systems studied, the active electrons included all π electrons, nonbonding (lone pair and unpaired) electrons, and in the case of transition states, any electrons involved in the forming or breaking of bonds. Similarly, the active space included the orbitals required to describe the minimal set of (bonding, nonbonding, and antibonding) π MO's, nonbonding orbitals, and any orbitals required to adequately describe the formation or breaking of bonds. The size of the active space thus depends on the species under study, but provided the active space contains all the MO's with occupation numbers that are substantially below 2 or above zero (say, approximately less than 1.95 or greater than 0.05), the CASPT2 energies vary little with the size of the active space. In practice this means some experimentation with the choice of active space in the CASSCF calculations to ensure that no potentially active orbital is forced to be inactive or secondary.

For species that could be adequately described by a single-reference wave function, the equilibrium geometries, vibrational frequencies, and energies were also determined by the G2-(MP2)[19] method, i.e., geometries and frequencies calculated at the MP2/6-31G(d) and SCF/6-31G(d) levels of theory but using CASSCF geometries and vibrational frequencies for the transition states. As in our previous work on pyrrole,[8,9] the CASSCF frequencies were scaled by a factor of 0.92.

Generally, the agreement between the results obtained by the CASPT2 and G2(MP2) methods was found to be reasonable. Where a large disagreement ($\sim$18 kJ mol^{-1} or more) was found, the energies and the Q_1 diagnostic were also computed at the QCISD(T)/cc-pVTZ level of theory at the CASSCF geometry to determine the source of the discrepancy and the adequacy of a single-reference treatment for a particular species. It has been noted[20] that for reactions involving changes in the number of electron pairs, there is a systematic error (for example, the singlet−triplet splitting in methylene is overestimated by $\sim$12 kJ mol^{-1}). However, exclusive use of a single-reference-based method, such as G2(MP2), is not adequate for studying the thermal decomposition pathways of furan because key intermediates could not be correctly described and thus some steps in the reaction schemes might be missed.

The rate constants for the reactions that are judged important in the overall thermal decomposition of furan were obtained using transition-state theory (TST).[21] The partition functions were calculated from the ab initio vibrational frequencies and rotational constants, using the standard expressions for quantum

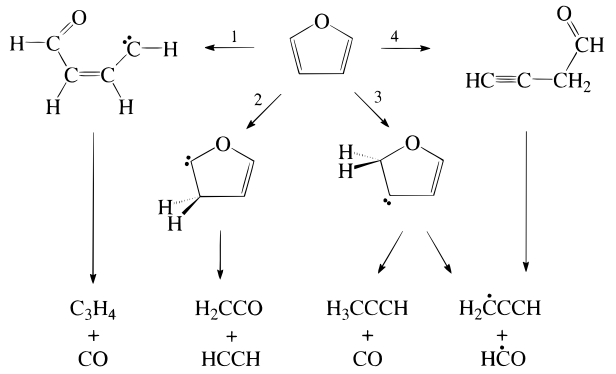

Figure 1. Unimolecular decomposition pathways of furan.

harmonic oscillators and rigid rotors.[22] In the case of very low frequency vibrational modes, the vibration was treated as a free rotor in two dimensions. Molecular entropies and heat capacities were also calculated from these partition functions.

For reactions without a barrier, variational transition-state theory (VTST)[23] was used. In such calculations the energies, rotational constants, and vibrational frequencies, and hence rate constants, were calculated at a set of geometries along the reaction coordinate (via successive small Newton−Raphson steps) at the CASSCF/cc-pVDZ level of theory. The energies were then scaled to give the correct CASPT2/cc-pVTZ dissociation energies. The transition state (at a given temperature) was then chosen as the point on the reaction coordinate that corresponds to the minimum value of the rate constant.

The computed rate constants, calculated over a range of temperatures (1100−1700 K), were then fitted to an Arrhenius form in order to determine the activation energies and preexponential, or *A*, factors.

The CASSCF geometry optimizations and frequency calculations were carried out using the DALTON[24] programs, which compute the gradients and Hessians analytically. The CASPT2 calculations were performed by using the MOLCAS[25] programs, while the Gaussian98[26] codes were used for the G2(MP2) and QCISD(T) calculations. The calculations were carried out on DEC Alpha 600/5/333 workstations of the theoretical chemistry group at the University of Sydney.

Computational Results

In this work we explored four distinct decomposition pathways (reactions 1−4) corresponding to the isomerization and subsequent decomposition of furan, yielding carbon monoxide, propyne, ketene, and acetylene as well as formyl and propargyl radicals as products, as summarized in Figure 1. In addition, we also computed the thermochemistry and rate constants of hydrogen abstraction from furan by methyl radicals. Although parts of the potential energy surfaces have been studied previously by Liu et al.,[11] their study is neither sufficiently comprehensive nor were the results obtained at a high enough level of theory to enable the calculation of reliable thermochemistry or kinetic parameters for the thermal decomposition pathways.

In the course of this computational study ∼45 molecular species (reactants, intermediates, transition states, and products) were studied by ab initio methods. The molecular geometries, computed at the CASSCF/cc-pVDZ level of theory, are given in Table 1S of the Supporting Information. Where variational TST was used to identify a transition state, the structure appropriate to 1400 K is reported. The absolute energies obtained at the CASPT2/cc-pVTZ, QCISD(T)/6-311G(d,p), QCISD(T)/cc-pVTZ, and G2(MP2) levels of theory and the zero-point vibrational energies are summarized in Tables 2S and 3S of the Supporting Information, while Table 4S contains the rotational constants and vibrational frequencies of structures **1**−**41**. Unless otherwise indicated, any reference to CASPT2 results in this paper implies the use of the cc-pVTZ basis. The relative energies calculated using these methods are shown in Tables 1 and 2. In subsequent sections of the paper the computed potential energy surfaces that show schematic structures of the molecular species (assigned the appropriate code **1**−**41**) and the energetics of the various pathways (as calculated at CASPT2/cc-pVTZ and G2(MP2) levels of theory) are shown as Figures 2−6.

Thermochemistry and Stability of Furan, L-Furan, and Furyl. Given its aromatic character, furan would be expected to have strong CH bonds. Thus, the extent of unimolecular CH fission could be expected to be insignificant under ∼1700 K. To validate this, we computed the CH bond enthalpy, viz. the enthalpy of the reaction

$$C_4H_4O\,(\text{furan}) \rightarrow C_4H_3O\,(\text{furyl}) + H, \quad \Delta_r H^0_{298} \qquad (1)$$

This was carried out by utilizing the experimental heats of formation of H, CH_3, and CH_4 along with our computed enthalpy of the isodesmic reaction

$$C_4H_4O + CH_3 \rightarrow C_4H_3O + CH_4 \qquad (2)$$

at 298 K. The isodesmic reaction enthalpies, corresponding to the formation of 2-furyl and 3-furyl (structures **2** and **3**) calculated from the isodesmic reaction, are 68.2 and 75.5 kJ mol^{-1}, respectively, when computed at the CASPT2 level. This leads to CH bond enthalpies of 506.3 and 513.6 kJ mol^{-1} for the two distinct CH bonds in furan. Interestingly, these bond enthalpies are unusually high, reflecting the thermodynamic instability of furyl. By comparison, the CH bond enthalpy in benzene is 469 kJ mol^{-1}. Therefore, in light of these high bond enthalpies unimolecular CH bond fission in the temperature range 1100−1700 K can be effectively ruled out.

The ground states of the furyls (**2** and **3**) are ^{2}A′, corresponding to the single electron in each isomer effectively occupying an in-plane sp^2 type hybrid orbital. It appears that the loss of a hydrogen atom makes little difference to the geometry of the remaining fragment. The OC′C and CC′C bond angles in 2- and 3-furyl are ∼3° larger than in furan (where C′ is the atom that loses the hydrogen), but the changes in bond lengths are generally less than 0.01 Å, with the exception of two OC distances that increased by ∼0.015 Å. Clearly, the removal of a hydrogen hardly changes the bonding. This is in contrast with the larger geometry changes that occur in analogous H loss reactions, for example, in ethylene, where according to our MP2/6-31G(d) computations, the CC bond decreases by 0.05 Å while the HC′C angle increases by 15°. By use of the G2(MP2) method, the lowest excited states (^{2}A″), with five π electrons, were computed to be just 60.2 and 105.2 kJ mol^{-1} above the ground states. In cyclopentadienyl and pyrrolyl the analogous five-π-electron $^2A_2$ states are actually the ground states.

An alternative bond cleavage that could occur in furan is the breaking of the CO bond, producing a linear carbene (L-furan). This is the reaction that was postulated to be rate-determining in the overall pyrolysis of furan by Organ and Mackie. According to our CASPT2 calculations, the ground state for this molecule (structure **4**) is ^{3}A″, lying 322 kJ mol^{-1} above furan at 0 K. When the CO bond was broken, the equilibrium CO distance was computed to be ∼2.90 Å, with the OCC and

TABLE 1: Relative Energies (Including Zero-Point Energy) at 0 K of Intermediates, Products, and Transition States (in kJ mol^{-1}) for the Unimolecular Decomposition of Furan

figure no. of PES	molecule/ structure	QCISD(T)/ 6-311G(d,p)	G2MP2	CASPT2/ cc-pVTZ	active space	QCISD(T)/ cc-pVTZ	Q_1 diagnostic
2	**1**	0	0	0	12/10	0	0.014
2	**4**	300	331	322	12/10		
2	**5**			371	12/10		
2	**8**	342	348	366	12/10	360	0.028
2	**9**			426	12/10		
2	**10**	297	326	316	12/10		
2	**11**			367	12/10		
2	**12**	345	350	341	12/10		
2	**13**			361	12/10		
2	**14**	210	240	225	12/10		
2	**15**			71	12/10		
2	**16**	369	388	324	12/10	319	0.031
2	**17**			406	12/10		
2	CO + **18**	276	327	333	8/6, 4/4	313	0.019, 0.032
2	CO + **19**			418	8/6, 4/4		
3	**20**	271	270	280	12/10		
3	**21**	223	229	264	12/10	229	0.020
3	**22**			304	12/10		
3	**23**			309	12/10		
3	**24**	337	346	352	12/10		
3	$CH_2CO + C_2H_2$	189	206	225	8/6, 4/4		
4	**25**	290	289	288	12/10		
4	**26**	244	245	279	12/10	248	0.024
4	**27**	244	245	264	12/10		
4	**28**	103	112	130	12/10	111	0.017
4	**29**	123	130	153	12/10	134	0.016
4	**30**	92	100	118	12/10	100	0.017
4	**31**	260	275	279	14/12		
4	$CO + CH_3CCH$	63	94	129	8/6, 4/4	91	0.019, 0.012
4	$CO + CH_2CCH_2$	70	97	128	8/6, 4/4	94	0.019, 0.013
4	$HCO + CH_2CCH$	391	424	414	7/5, 5/5		
5	**34**	360	352	356	12/10		
5	**35**	115	128	150	12/10	126	0.015
5	**36**	119	130	158	12/10	133	0.015
5	**37**	112	124	147	12/10	123	0.015

TABLE 2: Relative Energies (Including Zero-Point Vibrational Energy) at 0 K of Reactants, Products, and Transition States (in kJ mol^{-1}) for Hydrogen Abstraction by Methyl from Furan

figure no. of PES	molecule/ structure	QCISD(T)/ 6-311G(d,p)	G2MP2	CASPT2/ cc-pVTZ	active space
6	**1** + CH_3	0	0	0	12/10, 1/1
6	**41**	92	79	73	13/11
6	**42**	92	80	76	13/11
6	**2** + CH_4	72	73	62	13/11, 0/0
6	**3** + CH_4	74	74	68	13/11, 0/0

CCC angles opening up to ~125°. The CCH angle around the carbenic C atom is 129°, very close to the bond angle of 129.1° in methylene. The computed CO and CC bond lengths of 1.23, 1.47, and 1.39 Å are consistent with resonance between the Lewis structures:

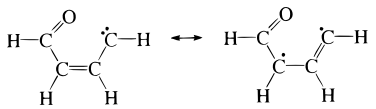

I II (3)

indicating a significant degree of delocalization of the π system. Thus, the bonding in ^{3}A″ L-furan is qualitatively different from that in furan. A CASSCF(8/7) study of L-furan by Wilsey et al.[10] yielded a structure similar to ours, with an energy of 274 kJ mol^{-1} above furan. This compares well with our CASSCF value of 279 kJ mol^{-1}, but clearly, the dynamic correlation effects on the energy of this bond fission reaction are substantial, as demonstrated by the CASPT2 results. The analogous bond fission in pyrrole is considerably more energetic; it was found to result in a triplet state some 393 kJ mol^{-1} above pyrrole. There is, however, a slightly more stable conformer of ^{3}A″ L-furan (structure **10**), which is obtained by a 180° rotation around the CC single bond. It is predicted to be 6 kJ mol^{-1} lower in energy than **4**. We did not, however, investigate other conformers of L-furan.

At the CASPT2 level, the ^{1}A′ state of L-furan (at the planar conformation of **4**) was found to lie 446 kJ mol^{-1} above furan at 0 K, although at the planar geometry two of its CASSCF vibrational frequencies are imaginary, corresponding to out-of-plane torsional modes. The ^{1}A″ state of L-furan on the other hand was found to be more stable, lying 370 kJ mol^{-1} above furan at 0 K with one low imaginary out-of-plane frequency. Relaxation of the planar symmetry restriction led to a slightly nonplanar structure (**5**) that was 371 kJ mol^{-1} above furan at the CASPT2 level, although the CASSCF energy (at the CASSCF optimized geometry) is 23 kJ mol^{-1} lower than for the planar ^{1}A″ state. The CASSCF wave function of this nonplanar singlet state is qualitatively quite similar to that of the ^{1}A″ state, with the two open-shell electrons occupying two different molecular orbitals that are effectively σ and π type and that are largely localized on the two different (C(3) and C(5)) carbon atoms, as in structure **II** in eq 3. The CC bond lengths (1.32, 1.46, and 1.46 Å) are also consistent with such localization, since they suggest a CC double bond (between C(4) and C(5)) and two single bonds. The finding that the lowest singlet state corresponds to a $\sigma^1\pi^1$ configuration (as for the triplet) rather than to σ^2 is unusual at first sight, since in the

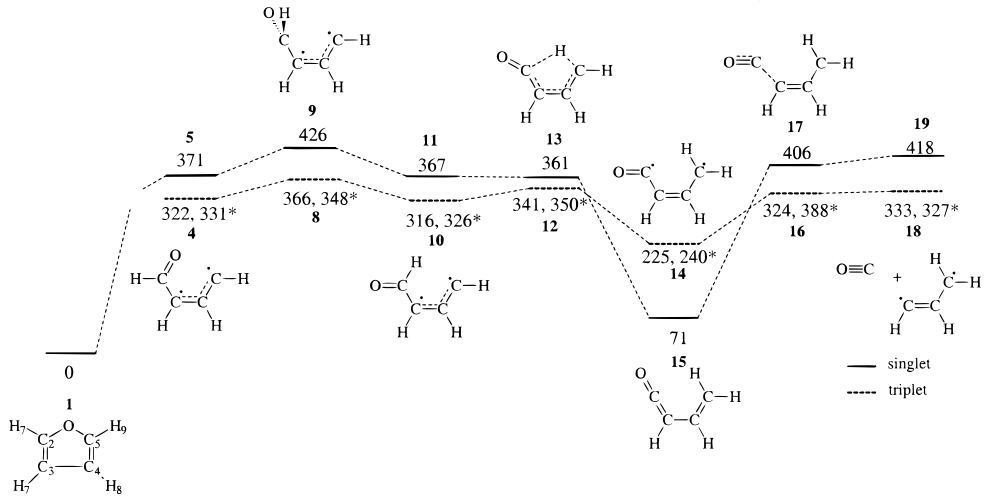

Figure 2. Potential energy surface for the formation of CO and vinylmethylene via ring opening of furan at 0 K. CASPT2 and G2(MP2) (*) energies are in kJ mol^{-1} relative to furan.

common C1 carbenes the opposite holds. We note, however, that similar behavior has been reported for vinylmethylene ($H_2C-CH=CH$).[27] Apart from the CC distances the largest difference between the geometries of the singlet and triplet states of L-furan is manifested in the slightly larger (133°) carbenic HCC bond angle in the singlet.

The major products of the decomposition of furan are C_3H_4, CO, C_2H_2, and ketene. Considering the reaction furan → C_3H_4 + CO (where C_3H_4 is either propyne or allene), the expected heats of reactions ($\Delta_r H^0_{298}$) based on experimental heats of formation are 110 and 113 kJ mol^{-1} for the propyne + CO and allene + CO paths, respectively. The computed CASPT2 heats of reactions are 139 and 138 kJ mol^{-1}, while at the G2(MP2) level they are 103 and 105 kJ mol^{-1}. In this particular application, where both reactants and products are closed-shell species, the G2(MP2) results are clearly superior to those obtained at the CASPT2 level, which appear to be in error by ~30 kJ mol^{-1} when compared with experimental values. The problem probably stems from an unbalanced description of the triply bonded product molecules in comparison with furan with two double bonds. As indicated by the results of Andersson,[20] the dissociation energies, viz., stabilities, of triply bonded diatomics, such as N_2, CO, and CN, are underestimated by the CASPT2 method by ~20−70 kJ mol^{-1}, but in general, the errors are significantly smaller for molecules with single and double bonds. A similar level of discrepancy is found also for the reaction furan → C_2H_2 + CH_2CO where the experimental heat of reaction (at 298 K) is 213.7 kJ mol^{-1}, while the corresponding CASPT2 value is 238 kJ mol^{-1} and while again the G2(MP2) result of 215 kJ mol^{-1} agrees well with experimental results.

Ring-Opening Reaction of Furan, Forming CO and C_3H_4. The previous kinetic modeling studies of the thermal decomposition of furan assumed that the initiation reaction is CO bond cleavage, producing L-furan, as summarized by pathway 1 in Figure 1. The kinetic parameters for this reaction were obtained by bond additivity assumptions. At that time, no ab initio quantum chemical results pertaining to this pathway were available. The study of the CO bond fission mechanism was therefore of high priority in our work.

Because most intermediates that contribute to this pathway, including L-furan, are biradicals, there are distinct singlet and triplet potential energy surfaces associated with this pathway, as shown schematically in Figure 2. The singlet and triplet surfaces cross in the neighborhood of systems whose ground states are closed-shell singlets. The overall rate constants for these decomposition reactions were estimated by two different approaches. The simplest method is to regard the species corresponding to the highest energy singlet and triplet barriers (**9** and **8**) as the transition states and to assume that once the system has passed those barriers, the reaction will go to completion. Alternatively, a rate constant is computed for each of the individual forward and reverse reactions that contribute to the overall decomposition of furan to CO and vinylmethylene by the ring-opening mechanism at a number of temperatures. This is followed by the solution of the resulting coupled differential equations (DE) at each temperature to obtain an overall rate constant. An Arrhenius fit of the resulting overall rate constants yields the usual activation energy and *A* factor in the temperature range of interest. In the case of the singlet pathway the results are effectively identical, with the rate constant at 1400 K computed to be 0.1 s^{-1} by both techniques. (The corresponding *A* factors and activation energies computed by the one-step and multiple-step (coupled DE's) methods are 2.4×10^{15} s^{-1}, 438 kJ mol^{-1} and 2.2×10^{15} s^{-1}, 437 kJ mol^{-1}, respectively, in the temperature range 1100−1700 K.) For the triplet pathway, the differences between the two approaches are more substantial, with the rate constants at 1400 K computed to be 15 and 7.6 s^{-1} by the one- and multiple-step methods. (The corresponding Arrhenius parameters are 1.8×10^{15} s^{-1}, 378 kJ mol^{-1} and 1.4×10^{15} s^{-1}, 382 kJ mol^{-1}, respectively.) The individual reactions and the nature of the participating species are discussed below. It is important to note, however, that irrespective of how these rate constants are estimated, they are very low in comparison with the computed rate constant of the alternative CO + C_3H_4 channel (see next section), and consequently, the simple ring fission of furan is not included in the kinetic model.

As discussed already, ring opening in furan occurs by CO bond fission, producing singlet and triplet L-furan. The lowest ^{1}A state (effectively a slightly distorted ^{1}A″ structure) was computed to be ~50 kJ mol^{-1} above the ^{3}A″ state. Because furan is a planar molecule, the ring-opening reaction, resulting in an eventual loss of the C_s symmetry, involves an avoided crossing between the (approximate) ^{1}A′ and ^{1}A″ states (in the reduced C_1 symmetry) at some long CO bond length. To study the bond cleavage, the energy of the system as a function of the (approximate) reaction coordinate was mapped out at the CASSCF/cc-pVDZ level of theory by optimizing the singlet

molecule in C_1 symmetry at a series of fixed CO distances. Because we were unsuccessful in our attempts to locate the reverse barrier to cyclization (**5** to **1**), we used variational transition-state theory for the calculation of the rate constant. Unfortunately, we were unable to obtain a smooth, continuous energy for the full range of distances studied. A discontinuity in the energy was encountered at a CO distance of ~2.705 Å. Species with a CO separation of 2.70 Å (structure **6**) or less were found to have electronic configurations that are very similar to furan's, whereby the CASSCF wave function is strongly dominated by a single configuration, while for species with a CO distance of 2.71 Å (structure **7**) or greater, the wave functions have biradical character, as in **5**, with two equally dominant configurations with singly occupied MO's that are effectively σ and π type. The resulting ^{1}A state thus has the characteristics of a ^{1}A″ state. The apparent discontinuity is probably due to the active space in the CASSCF wave functions not being large enough so that as the character of the wave function changes, the optimization procedure locates two distinct local minima with respect to rotations in the orbital and configuration parameter spaces. As one may expect, the discontinuity in the energy is accompanied by substantial changes in the bond lengths, as revealed by a comparison of the geometries of **6** and **7** (see Table S1), as well as a discontinuity in the computed rate constants. After some thought, the transition state for this reaction was chosen to be structure **6**, i.e., located at the CO distance of 2.70 Å. The calculated rate constants that were thus obtained, after scaling the CASSCF energies to yield the correct bond fission energy, were a factor of 10−50 higher (depending on temperature) than the rate constants that were obtained by choosing **7** as the transition state. Given the discontinuous jump in the energy, it is conceivable that the energy of **7** may be biased and not properly reflect the true energy difference between transition state and reactant, so **6** may well be a more realistic choice. More importantly, however, in the context of this work, i.e., the elucidation of the decomposition mechanisms of furan, an upper bound to the rate of this ring-opening reaction is sufficient to determine whether the ring-opening reaction is likely to contribute at all and thereby help in the identification of the dominant mechanisms. The rate constants obtained with **6** as the transition state will certainly represent an upper bound, but as discussed above, under these circumstances the rate-determining step will be the internal rotation of the formyl group, which is sufficiently energetic in an absolute sense to render the ring-opening reaction unimportant. Wilsey et al.[10] located a conical intersection between the ^{1}A′ and ^{1}A″ surfaces at a CO distance of 2.51 Å, some 397 kJ mol^{-1} above furan. The discrepancy between the two studies may be due to the imposition of planarity in the work of Wilsey et al.[10] and/or the smaller active space in their study.

For the analogous reaction producing L-furan in the triplet ground state, i.e., **1** → **4**, the transition state was chosen to be structure **7** (with a CO separation of 2.71 Å), since this was judged to be a reasonable approximation to the singlet/triplet crossing point. (The triplet energy of **7** is just 7 kJ mol^{-1} below the singlet energy, while for **6** the triplet state is 54 kJ mol^{-1} above the singlet, as computed at the CASSCF/cc-pVDZ level.) As in the case of ring-opening on the singlet surface, the resulting rate constant can be regarded as an upper bound, especially since it is obtained by simple transition-state theory, without explicit inclusion of the spin−orbit coupling mechanism that allows the intersystem crossing to occur. Note that despite the obvious similarities, the ring-opening reaction in pyrrolenine (2H-pyrrole) is quite different because of the presence of an extra hydrogen atom in the latter that results in a different type of biradical, namely, N═CH−CH−CH−CH_2.

Rotation about the formyl group around the CC single bond is quite facile in both the singlet and triplet species, although, as remarked above, the barriers associated with that rotation, viz., 426 and 366 kJ mol^{-1}, respectively (at the CASPT2 level), are actually the highest on both the singlet and triplet surfaces. Interestingly, **9** is described effectively by a closed-shell wave function and fairly well-defined single and double bond alternation (in contrast with the biradical **5**). Presumably, a certain amount of conjugation with the C═O bond occurs in **5**, which is near-planar, but the delocalization of the unpaired π electron in **9** is not possible to the same extent. The intermediates **10** and **11** are again planar, with bond lengths and electronic structures that are effectively the same as for the corresponding isomers **4** and **5**, respectively.

The facile 1,4-H-transfers from the formyl group to the end carbon of **10** and **11**, resulting in vinyl ketene (**14** and **15**), are qualitatively similar to the H-transfer in the pyrrolic system that yields *cis*-crotononitrile. Although it appears that transition state **13** is lower in energy than **11**, at the CASSCF level at which the geometries were optimized, **13** was in fact ~10 kJ mol^{-1} higher than **11** and had a single imaginary frequency corresponding to the reaction coordinate. This suggests that the H-transfer in the singlet state is very facile, with a low barrier, but at the CASPT2 level it is either underestimated or occurs at a somewhat different geometry. It is worth noting also that in contrast with the triplet transition state **12** the singlet **13** is quite nonplanar. The ^{1}A′ ground state of vinyl ketene (**15**) has a closed-shell configuration, and because it is predicted to be thermodynamically quite stable, it may well be observed experimentally. The ^{3}A″ excited state (**14**) is a biradical, the two unpaired electrons being effectively localized in σ and π MO's as indicated by their Lewis structures in Figure 2. The CC bond lengths (1.47, 1.40, and 1.38 Å) in **14** indicate, however, that there is considerable delocalization of the unpaired π electron.

CC bond cleavage in these two molecules leads to the products CO and vinyl methylene. Although transition states for these reactions (**16** and **17**) were found at the CASSCF/cc-pVDZ level, the barriers to recombination are likely to be very small because they seem to disappear when their heights are recalculated at the CASPT2 level. A fairly large discrepancy (64 kJ mol^{-1}) is also noted on comparing the G2(MP2) and the CASPT2 energies for the triplet transition state **16**, although the latter agrees well with the QCISD(T)/cc-pVTZ result. As the results in Table 1 suggest, the above discrepancy is most likely caused by the use of MP2 theory to correct for basis set deficiencies in the G2(MP2) calculation. The Q_1 diagnostic for the QCISD(T)/cc-pVTZ wave function is also quite large at 0.031, which is indicative of some near-degeneracy problems. This is not surprising in light of the fairly large CC distance that corresponds to the breaking bond. Thus, the CASPT2 results are expected to be the most reliable in this situation.

Vinyl methylene (**18**, **19**) can readily isomerize to propene or allene. A detailed study of these reactions has been carried out by Yoshimine et al.[27] The products on the triplet potential energy surface were found to be 333 kJ mol^{-1} above furan at 0 K, while the singlet products were found to be 418 kJ mol^{-1} above furan (i.e., the reaction **15** → CO + singlet vinylmethylene was found to be 347 kJ mol^{-1} endothermic.)

Wilsey et al.[10] also located a pathway from the biradical **5** to acylcyclopropene, whose energy was calculated to be 247 kJ

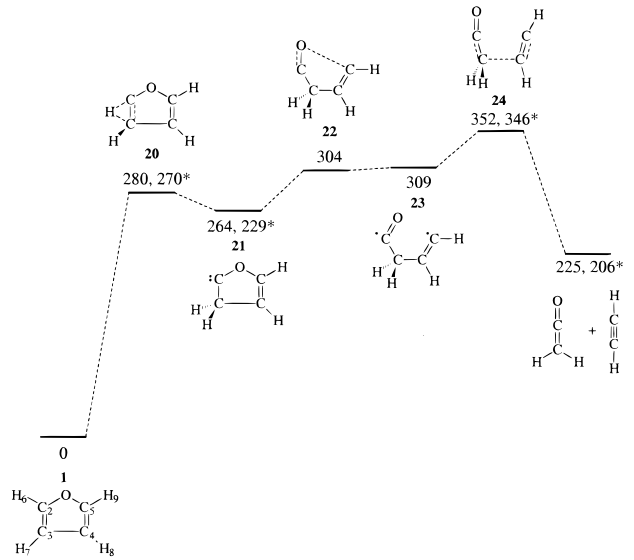

Figure 3. Potential energy surface for the formation of ketene and acetylene via a cyclic carbene intermediate at 0 K. CASPT2 and G2(MP2) (*) energies are in kJ mol^{-1} relative to furan.

mol^{-1} above furan. Although they were not able to locate a transition state for the ring closure, it was estimated to lie higher than 340 kJ mol^{-1} above furan. The subsequent decomposition of acylcyclopropene could occur by a concerted 1,2-H migration and CC bond fission (with an energy barrier that is likely to be >100 kJ mol^{-1} above acylcyclopropene) to produce CO and cyclopropene or via CC bond fission to produce HCO and cyclopropenyl radicals (with an endothermicity of >500 kJ mol^{-1} above furan). Because of their high energies, these pathways were not considered in the computation of the overall rate constant in our study.

Formation of Ketene and Acetylene via a Cyclic Carbene Isomer of Furan. This pathway (number 2 in Figure 1) involves a 1,2-hydrogen migration that results in a cyclic carbene intermediate followed by two successive bond cleavages, yielding ketene and acetylene as products. The potential energy surface for this decomposition process is shown in Figure 3. There are three transition states, and we can obtain the overall rate constant either by a one-step approach, regarding the CC bond-breaking reaction as rate-determining, i.e., choosing **24** as the transition state, or as described in the previous section by solving the coupled DE's of the multistep process. The resulting rate constants computed by the one- and multistep methods are 431 and 234 s^{-1} at 1400 K, respectively. (The corresponding Arrhenius parameters are 3.3×10^{16} s^{-1}, 372 kJ mol^{-1} and 1.5×10^{15} s^{-1}, 344 kJ mol^{-1}, respectively, in the temperature range 1100−1700 K.)

The first transition state (**20**) associated with the initial 1,2-H-migration step leading to the cyclic carbene intermediate (**21**) corresponds to a relatively low barrier of 280 kJ mol^{-1}. In the transition state the migrating hydrogen is near-perpendicular to the plane of the ring and is located slightly closer to the carbon it is moving from (C(2)) than the one it is moving to (C(3)). There is also a concomitant increase in the OC(2) and C(2)C(3) bond lengths. The carbene intermediate (**21**) is of C_s symmetry, and the ground state is ^{1}A′. The CASPT2 and G2(MP2) estimates of the barrier height are within 10 kJ mol^{-1} of each other, but a significantly larger difference is evident in the case of the carbene, with the G2(MP2) relative energy being 35 kJ mol^{-1} lower than the CASPT2 value. While some of this discrepancy may be due to inaccuracies in the CASPT2 treatment, the somewhat high value of the Q_1 diagnostic for the carbene (0.02 in the QCISD(T)/cc-pVTZ calculations) suggests that there may be some near-degeneracy problems in the QCI calculations. Analogous discrepancies were noted in the case of the cyclic carbenes for pyrrole too, although for the latter the differences between the CASPT2 and G2(MP2) energies were ∼22 kJ mol^{-1} or less. In the computation of the rate constant by the multiple-step method the CASPT2 value was used, although it should be noted that the choice of energy for the carbene intermediate in this scheme does not affect significantly the value of the overall rate constant. The structure of the carbene (**21**) appears to be fairly well represented by the Lewis structure in Figure 3 with respect to the CC single and double bonds, but there is obviously a significant double bond character to the bond between the carbenic carbon and oxygen as a result of the donation of O lone pair density into the formally empty p_π orbital on the carbon, resulting in an OC(2) bond length of 1.33 Å. The OC(2)C(3) bond angle of 105.8° is consistent with the 1A′ state of a carbene. By comparison, the OC(5)C(4) bond angle is 110.6°, which is nearly the same as the angle in furan.

The ring opening of the carbene occurs by cleavage of the OC(5) single bond via transition state **22**, which then yields a biradical intermediate (**23**). In the transition state the length of the breaking bond was found to be ∼2.0 Å, with the remaining CO bond having effectively shortened to a double bond and the OC(2)C(3) angle having increased to ∼117°. The biradical intermediate is characterized by a C···O distance of ∼2.3 Å and essentially two singly occupied in-plane orbitals localized on C(2) and C(5). At the CASPT2 level the transition state (**22**) appears to be more stable than the biradical (**23**), but as in other cases already commented on, at the CASSCF level (at which the geometries were optimized) the transition state was found to have a (slightly) higher energy than the biradical as well as a single imaginary frequency corresponding to the expected ring-opening mode.

Finally, the C(3)C(4) bond cleavage in biradical **23**, via transition state **24**, yields the products ketene and acetylene. The breaking CC bond distance in this transition state was computed to be ∼1.9 Å, with the two fragments effectively assuming the geometries of the products. As noted above, this final reaction is the rate-determining one. The critical energy associated with the transition state (**24**) was computed to be 352 kJ mol^{-1} above furan at the CASPT2 level of theory, in close agreement with the G2(MP2) prediction. Overall, the decomposition reaction of furan to ketene and acetylene is found to be 225 kJ mol^{-1} endothermic at 0 K at the CASPT2 level, while G2(MP2) predicts a lower value of 206 kJ mol^{-1}. These values actually bracket the experimental heat of reaction, which (at 298 K) is 214 kJ mol^{-1}.

The previous study of this pathway by Liu et al.,[11] having failed to identify the biradical intermediate **23**, implied that ketene and acetylene are formed as a result of a concerted one-step dissociation of the carbene intermediate (**21**). Their transition state for that process is, however, essentially identical to **24**, which, as shown in this work, corresponds to the CC bond fission of the biradical **23**. Because Liu et al.[11] carried out the geometry optimizations using density functional theory, it is not surprising that **23** was not located because it can only be characterized by methods based on at least a two-determinant reference state. In fact, in our G2(MP2) study of this pathway, the UHF and UMP2 geometry optimizations of **23** simply collapsed onto **21**. Otherwise, the reported energetics of Liu et al.[11] for this pathway are comparable with our G2(MP2) results.

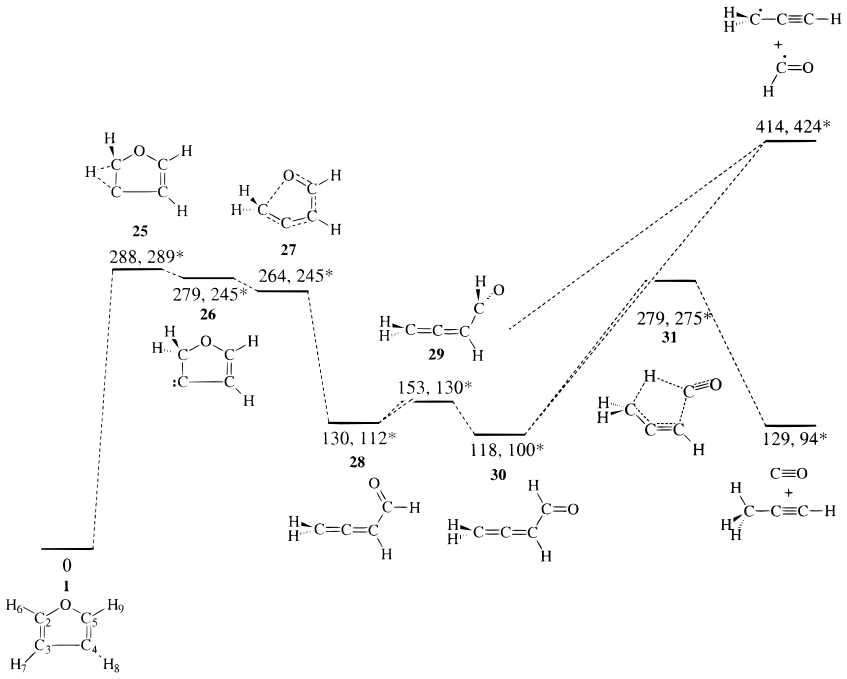

Figure 4. Potential energy surface for the formation of CO and propyne (and formyl and propargyl radicals) via a cyclic carbene intermediate at 0 K. CASPT2 and G2(MP2) (*) energies are in kJ mol^{-1} relative to furan.

They also considered a pathway from carbene **21** to propyne and CO. The critical barrier for that reaction was computed to be 400 kJ mol^{-1} relative to furan. Because there is a much more favorable route to the production of those products, as discussed in the next section, this high-energy pathway has not been pursued in our study.

Formation of Carbon Monoxide and Propyne via a Cyclic Carbene Isomer of Furan. This pathway (number 3 in Figure 1) involves an alternative type of 1,2-hydrogen migration compared to that considered before, resulting in an another cyclic carbene intermediate, which, on ring opening, yields CO and propyne or formyl and propargyl radicals as products. The computed potential energy surfaces for these reactions are shown in Figure 4. These reactions are modeled by assuming that the formyl allene (**28**) will be thermally stabilized and will subsequently decompose as a result of further collisional activation. The rate constant for the furan → formyl allene (**28**) reaction was obtained by assuming that the rate-determining step is the initial 1,2-H transfer, since the subsequent CO bond fission is considerably more facile. When **25** is identified as the transition state, the resulting *A* factor and activation energy are 5.94×10^{13} s^{-1} and 294.1 kJ mol^{-1}, respectively (in the temperature range 1100−1700 K).

The decomposition of formyl allene (**28**) then takes place by a concerted reaction of its rotamer (**30**) in which a 1,4-hydrogen transfer and simultaneous CC bond fission occur. The latter is clearly the rate-determining step, and on the basis of the CASPT2 results, the Arrhenius *A* factor and activation energy were calculated to be 1.66×10^{13} s^{-1} and 167.9 kJ mol^{-1} (in the temperature range 1100−1700 K). Alternatively, CC bond fission in **28** and **30** could yield the propargyl and formyl radicals. By use of variational transition-state theory, as discussed below, the *A* factors and activation energies of these two reactions were computed to be 1.45×10^{15} and 7.94×10^{14} s^{-1}, and 289.0 and 292.3 kJ mol^{-1}, respectively (in the temperature range 1100−1700 K).

As noted above, in these two-step processes the rate-determining initial step is the formation of a cyclic carbene (**26**). As in the case of another carbene (**21**), the G2(MP2) as well as the QCISD(T) results differ from the CASPT2 predictions by over 30 kJ mol^{-1}. Because the energy of this intermediate does not come into the computation of the rate parameters, we have not yet attempted to rigorously resolve the above inconsistency, although we note that in this instance too the somewhat large value of the Q_1 diagnostic, viz., 0.023, suggests the possibility of near-degeneracy problems in the QCI calculations. The bond lengths and angles in **26** are as one may expect in a carbene, with noticeable π delocalization resulting in a noticeably short CO bond flanking the CCC π system. The CO bond fission in the carbene that involves a simultaneous rearrangement of the π system is evidently very facile. A barrier to this process, corresponding to the transition state **27**, was located at the CASSCF level of theory, but it may well be nonexistent at a more highly correlated level. The product of this reaction is a rotamer of formyl allene (**28**), a molecule with C_s symmetry and a planar backbone of heavy atoms. It can readily isomerize to its rotamer (**30**) and then decompose to propyne and carbon monoxide in a concerted reaction via transition state **31**. This transition state was found to have a fairly long breaking CC bond of 1.78 Å, with the migrating hydrogen being approximately equidistant from C(5) and C(2) (∼1.4 Å) and the C(2)C(3)C(4) chain assuming a bent configuration with an angle of 126°. By use of the intrinsic reaction coordinate (IRC) approach at the CASSCF level of theory, it was confirmed that **31** is indeed the transition state for this decomposition step. The barrier associated with this reaction step is actually slightly lower than the one in the initial furan → carbene (**26**) step, and consequently, the second reaction in the pathway, viz., the decomposition of the formyl allene intermediate (**28**), is predicted to be very fast, as the Arrhenius parameters above indicate.

The above reaction is a 1,4 sigmatropic rearrangement and decomposition, whereby the migration of the CH σ bond is accompanied by the simultaneous rearrangement of the in-plane π electrons and the breaking of σ bond that connects the formyl and allene fragments in the reactant, as shown below:

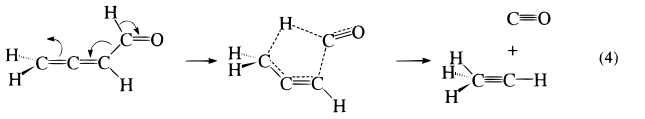

(4)

This reaction is a close analogue of the 1,5 sigmatropic reaction of allene imine, which was found to play a key role in the pyrolysis of pyrrole,[8,9] although in the latter it is the N-bound hydrogen that migrates, giving rise to a six-atom cyclic transition state:

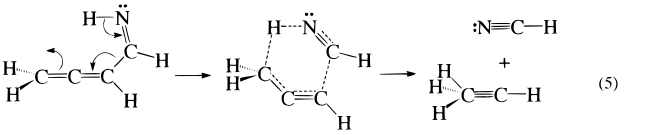

(5)

A closer analogue of reaction 4 with a five-atom cyclic transition state is an alternative decomposition pathway of allene imine, where the C-bound hydrogen migrates, resulting in HNC and propyne as products:

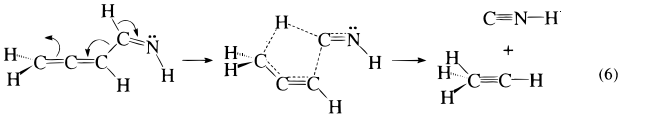

(6)

However, because the transition state in reaction 6, computed at the CASPT2 level, lies ~82 kJ mol^{-1} above that in reaction 5 (i.e., ~414 kJ mol^{-1} above the original reactant, viz., pyrrole), this last pathway is not part of the kinetic model developed for the pyrolysis of pyrrole. Interestingly, however, while transition state **31** lies only ~275 kJ mol^{-1} above furan, the barriers for the propyne + CO, propyne + HCN, and propyne + HNC recombination reactions are comparable at 181, 135, and 156 kJ mol^{-1}, respectively.

The results of Liu et al.[11] are in qualitative agreement with ours with respect to the mechanism of conversion of furan to the carbene intermediate (**28**), but in their study the isomerization of **28** to **30** was skipped, and therefore, the crucial transition state (**31**) leading to the products was not found either. Liu et al.[11] considered two alternative pathways leading to the production of propyne + CO and allene + CO, but the high energies of the appropriate transition states (322 and 421 kJ mol^{-1}, respectively) effectively rule these out as viable alternatives to the pathway proposed in this work.

We note that in the case of the formyl allenes (**28**−**30**) there appears to be a systematic discrepancy of ~20 kJ mol^{-1} between the CASPT2 and G2(MP2) relative energies. The latter energies are in good agreement with the QCISD(T)/cc-pVTZ results, and moreover, in this instance the Q_1 diagnostics for these species suggest that QCI should be reliable. A similar level of discrepancy was noted for the analogous allenic imine systems in our previous work on the thermal decomposition of pyrrole. At this stage we do not have an explanation for this discrepancy as well as those already commented on, but note that the choice of energies for these molecules has virtually no effect on the kinetic model. The rate parameters quoted above were obtained from the CASPT2 data.

Loss of HCO from **28** and **30** via C(5)C(4) bond fission to produce the propargyl and formyl radicals was also studied. These reactions were found to be 284 and 296 kJ mol^{-1} endothermic, respectively (at the CASPT2 level), and because these reactions do not have a reverse barrier, variational transition-state theory was used to identify the transition states (**32** and **33**) and to compute the rate parameters quoted above.

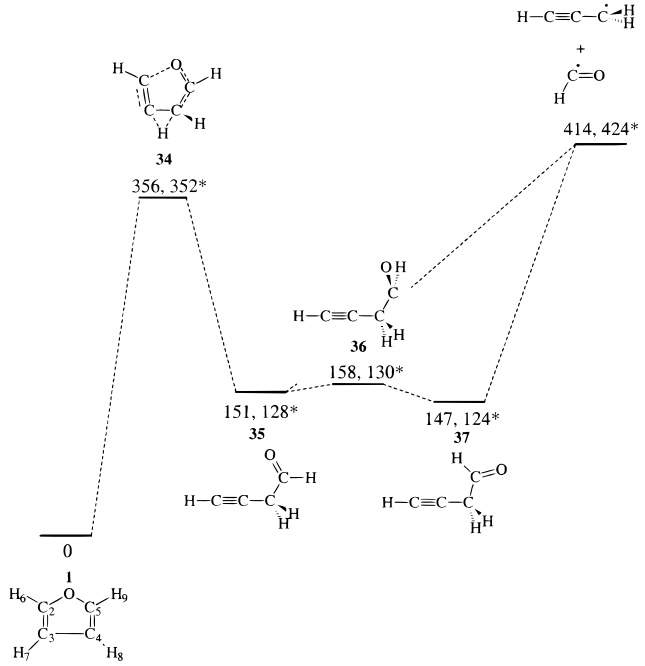

Figure 5. Potential energy surface for the formation of formyl and propargyl radicals via a formyl propyne intermediate at 0 K. CASPT2 and G2(MP2) (*) energies are in kJ mol^{-1} relative to furan.

The resulting critical CC distance, corresponding to the breaking bond in transition state **32**, ranges from 2.60 Å (1700 K) to 2.62 Å (1100 K), while the corresponding distance in **33** varies from 2.57 Å (1700 K) to 2.58 Å (1100 K).

In addition to the pathways discussed above, we also investigated two other possible decomposition pathways of **28** and **30** in order to determine important pathways in the thermal decomposition of furan. The first of these is the 1,2-H migration of a hydrogen to the oxygen, forming a carbene intermediate, followed by its isomerization to the cis rotamer and subsequent 1,5 sigmatropic hydrogen shift that produces propyne and CO:

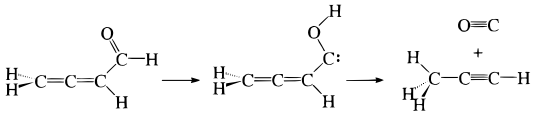

(7)

The critical energy of the first 1,2-H shift step of this reaction was found to be too high in energy (~460 kJ mol^{-1} above furan at 0 K) to allow this scheme to be competitive with the one discussed above. As remarked above, the 1,5 sigmatropic H-shift step is a key component of the HCN + propyne channel in the pyrolysis of pyrrole,[8,9] but there, the intermediate is a stable allenic imine rather than a carbene, as in the case of furan. The other alternative pathway is the concerted 1,2-H migration from the formyl carbon and CC bond fission to yield CO and allene:

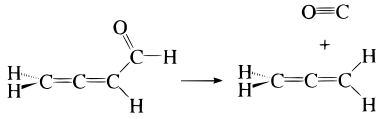

(8)

The critical energy of this reaction, viz., 436 kJ mol^{-1}, was also considered too high to warrant its inclusion in the kinetic model.

Formation of Formyl and Propargyl Radicals via Formyl Propyne. This pathway (number 4 in Figure 1) is summarized in Figure 5. It involves a 1,2-H migration from C(3) to C(4) with simultaneous C(2)O bond fission via transition state **34**,

producing formyl propyne (**35**) which has C_s symmetry with a planar backbone of heavy atoms. In contrast with the previous 1,2-H migrations that produced cyclic carbenes, in this case no cyclic carbene structure could be located on the potential energy surface. Although the transition state **34** appears to be leading to a ring structure, relaxation of the geometry along the intrinsic reaction coordinate toward the product resulted in CO bond fission and formyl propyne as product. In the transition state (**34**) the migrating hydrogen was found to be 1.37 Å from C(3) and 1.21 Å from C(4), with the "breaking" C(2)O bond length being 1.41 Å. By comparison, the nonbreaking C(5)O bond distance was computed as 1.33 Å, only ~0.05 Å shorter than in furan. The barrier height for this step was found to be 356 and 352 kJ mol^{-1} at 0 K at the CASPT2 and G2(MP2) levels of theory, respectively. The resulting *A* factor and activation energy for the furan → formyl propyne (**35**) reaction was computed to be 1.06×10^{14} s^{-1} and 363.9 kJ mol^{-1}, respectively (in the temperature range 1100−1700 K). In contrast with the above results, the analogous CH and CO distances in this transition state, obtained by a B3LYP/6-31G(d,p) calculation as reported by Liu et al.,[11] are 1.15, 1.73, 3.7, and 1.23 Å. The barrier at that geometry was computed to be 392 kJ mol^{-1} in a QCISD(T)/6-311++G(d,p) calculation. We attribute the large discrepancy between the two calculations to the poor performance of DFT in describing this transition state, producing a molecule that has the appearance of a singlet carbene.

As found in the case of the formyl allene molecules (**28**, **30**), there is only a small barrier separating the two conformers of formyl propyne (**35**, **37**). Also, as one may expect, the allene and propyne isomers have comparable stabilities. A 1,5 sigmatropic H shift in **37** could result in the formation of allene and CO, but contrary to our initial expectations, on the basis of our findings for the analogous reaction in pyrrole, the CASPT2 critical energy for this reaction, viz., 445 kJ mol^{-1} above furan, is too high for this pathway to contribute to the allene + CO channel. Liu et al.[11] reported transition states at energies of 422 and 642 kJ mol^{-1} above furan for the **35** → CO + propyne and **37** → CH_2CO + C_2H_2 reactions, respectively, by concerted H migration and CC bond fission. Again, in light of the more favorable pathways already found, neither of these channels located by Liu et al.[11] are expected to contribute appreciably to the appropriate rate constants.

The CC bond fission reaction in the two formyl propynes was studied using variational transitional-state theory. The resulting *A* factors and activation energies, based on the CASPT2 results, are 1.78×10^{15} and 1.05×10^{15} s^{-1}, and 253.3 and 252.0 kJ mol^{-1} (in the temperature range 1100−1770 K) for the bond fission from **35** (via transition state **38**) and **37** (via transition state **39**), respectively. The CC distances characterizing the breaking CC bonds were found to be 2.63−2.80 Å.

Hydrogen Abstraction by Methyl Radical. Given the presence of a considerable quantity of methyl radicals in the reaction mixture, as indicated by the kinetic modeling and also by the experimental observation of significant amounts of methane in the products, the importance of hydrogen abstraction from furan by methyl needs to be assessed. The computed reaction pathways are summarized in Figure 6. There are two distinct hydrogens that can be abstracted, resulting in the two distinct furyl isomers (**2**, **3**), via the transition states **40** and **41**. As the results show, the energetics of these two reactions are comparable. The barriers were computed to be 73 and 76 kJ mol^{-1}, respectively, with the reactions being 62 and 68 kJ mol^{-1} endothermic (all at 0 K). The resulting *A* factor and activation energy for the combined formation of **2** and **3** are 9.7×10^{13} s^{-1} and 96.9 kJ mol^{-1} (in the temperature range 1100−1700 K). The reverse barriers are only 6−8 kJ mol^{-1}, indicating the ease with which the reverse reaction, viz., H abstraction from methane by furyl, can occur.

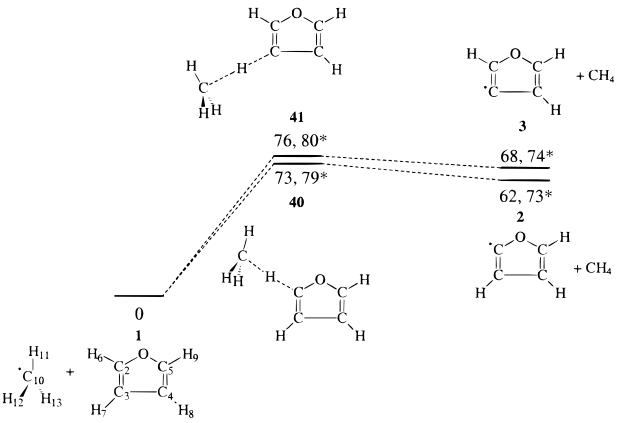

Figure 6. Potential energy surface for hydrogen abstraction by methyl radicals from furan at 0 K. CASPT2 and G2(MP2) (*) energies are in kJ mol^{-1} relative to furan + methyl.

The abstraction process is similar to hydrogen abstraction by methyl from ethylene.[12] In both systems the critical CH distances corresponding to the breaking and forming CH bonds are 1.37 and 1.27−1.30 Å, respectively. Because the geometric parameters in the furyls and furan are very close, the only significant change in furan that occurs during the abstraction is the lengthening of the breaking CH bond. This is in some contrast with the abstraction process in ethylene, where the CC bond length decreases from 1.33 to 1.29 Å while the CCH angle increases from 121.3° to 128.8°. This results in a tighter transition state for the abstraction from ethylene and hence a lower *A* factor than for the analogous abstraction from furan. Because rotation of the methyl group about the CHC bond in the transition state is essentially unhindered (with harmonic vibrational frequencies of ~17 cm^{-1}), this mode was treated as a free rotor in this work. A similar low-frequency mode was observed in the study of ethylene, but because there it was treated as a vibrational frequency, no useful comparison between the *A* factors obtained in this work for furan and the *A* factors extracted from the ethylene work can be made.

Summary of Computational Results. Ab initio methods have been used to study four distinct reaction pathways that describe the unimolecular decomposition of furan, as well as a secondary bimolecular decomposition mechanism. To determine the important mechanisms, it is instructive to compare the computed rate constants for each of these pathways at an intermediate temperature in relation to the experimental studies, such as 1400 K. When the disappearance of furan was examined at that temperature, the upper bound to the rate constant for the ring-opening reaction of furan on the singlet surface, yielding vinyl ketene (**15**), was computed to be 0.1 s^{-1} while the corresponding value for the triplet surface, resulting in CO + vinylmethylene (**18**), was estimated to be 7.6 s^{-1}. The rate constant for the reaction that leads to the formation of ketene and acetylene via a cyclic carbene intermediate (see Figure 3) was computed to be 234 s^{-1}. The largest rate constant, viz., 629 s^{-1}, was obtained for the reaction that results in formyl allenes (**28**, **30**) as stable intermediates (see Figure 4), while the rate constant for the reaction yielding formyl propynes (**35**, **37**) was found to be 2.8 s^{-1}. From these data, it is clear that the reactions involving 1,2-H migrations, which lead to the cyclic carbenes (**21** and **25**), are by far the most important unimolecular

TABLE 3: Kinetic Model for Furan Pyrolysis

	reaction[a]	A[b]	n	E_a[b]	ref		reaction[a]	A[b]	n	E_a[b]	ref
1	furan + CH_2 ⇔ CH_3 + furyl2	2.00×10^{12}	0	33.5	est[c]	42	$CH_2 + CH_4 \leftrightarrow 2CH_3$	2.46×10^{6}	2	34.6	28
2	furan + CH_3 ⇔ CH_4 + furyl2	9.60×10^{13}	0	87.9	PW/abin[c]	43	$C_2H_3 + C_2H_4 \leftrightarrow C_4H_6 + H$	6.30×10^{11}	0	13.0	44
3	furan + H ⇔ H_2 + furyl2	2.00×10^{14}	0	75.3	est	44	$CH_3 + CH_2CO \leftrightarrow C_2H_5 +$ CO	4.00×10^{11}	0	0.0	see text
4	furyl2 ⇔ CO + C_3H_3	1.00×10^{14}	0	104.6	est	45	H + $C_3H_4P \leftrightarrow CH_3 + C_2H_2$	1.30×10^{5}	2.5	4.2	29
5	furan ⇔ furop1	5.90×10^{13}	0	292.9	PW/abin	46	H + $C_3H_4P \leftrightarrow H_2 + C_3H_3$	1.00×10^{12}	0	26.4	45
6	furop1 ⇔ furop2	2.20×10^{12}	0	23.6	PW/abin	47	$CH_3 + C_3H_4P \leftrightarrow CH_4 +$ C_3H_3	2.00×10^{12}	0	32.2	45
7	furop1 ⇔ HCO + C_3H_3	1.40×10^{15}	0	289.1	PW/abin	48	$C_4H_4 \leftrightarrow 2C_2H_2$	1.48×10^{15}	0	345.2	46
8	furop2 ⇔ HCO + C_3H_3	7.90×10^{14}	0	292.5	PW/abin	49	$C_4H_4 \leftrightarrow C_4H_2 + H_2$	2.00×10^{14}	0	364.0	46
9	furop2 ⇔ CO + C_3H_4P	1.70×10^{13}	0	167.8	PW/abin	50	C_2H_5 (+M) ⇔ C_2H_4 + H (+M)	2.00×10^{13}	0	166.0	28
10	furan ⇔ C_2H_2 + CH_2CO	9.00×10^{14}	0	344.3	PW/abin	51	C_2H_4 (+M) ⇔ C_2H_2 + H_2 (+M)	8.00×10^{12}	0.4	371.4	28
11	HCO + M ⇔ H + CO + M	1.60×10^{14}	0	65.9	36	52	H + C_2H_3 (+M) ⇔ C_2H_4 (+M)	6.08×10^{12}	0.3	1.2	28
12	HCO + H ⇔ H_2 + CO	2.16×10^{14}	0	0.0	37	53	C_2H_4 + H ⇔ C_2H_3 + H_2	5.01×10^{13}	0	33.5	28
13	HCO + CH_3 ⇔ CO + CH_4	1.20×10^{14}	0	0.0	38	54	$C_2H_3 + C_2H_3 \leftrightarrow C_4H_6$	3.00×10^{13}	0	0.0	29
14	HCO + C_2H ⇔ C_2H_2 + CO	6.00×10^{13}	0	0.0	38	55	H + C_2H_2 (+M) ⇔ C_2H_3 (+M)	1.00×10^{13}	0	11.3	28
15	HCO + C_2H_3 ⇔ C_2H_4 + CO	9.00×10^{13}	0	0.0	38	56	$2CH_3$ (+M) ⇔ C_2H_6 (+M)	3.60×10^{13}	0	0.0	28
16	HCO + C_2H_5 ⇔ C_2H_6 + CO	4.30×10^{13}	0	0.0	39	57	C_2H_6 + H ⇔ H_2 + C_2H_5	5.37×10^{2}	3.5	21.8	28
17	HCO + CH_2 ⇔ CH_3 + CO	1.80×10^{13}	0	0.0	38	58	$C_2H_6 + CH_3 \leftrightarrow CH_4 +$ C_2H_5	5.50×10^{-1}	4	34.7	28
18	HCCO + H ⇔ CH_2 + CO	1.50×10^{14}	0	0.0	40	59	$CH_3 + H_2 \leftrightarrow CH_4$ + H	6.46×10^{2}	3	32.2	28
19	HCCO + C_2H_2 ⇔ CO + C_3H_3	1.00×10^{10}	0	0.0	41	60	CH_3 + H (+M) ⇔ CH_4 (+M)	6.00×10^{16}	−1	0.0	28
20	2HCCO ⇔ 2CO + C_2H_2	1.00×10^{13}	0	0.0	28	61	C_2H_5 + H ⇔ $CH_3 + CH_3$	1.00×10^{14}	0	0.0	28
21	$CH_3 + C_2H_4 \leftrightarrow C_2H_3 + CH_4$	2.27×10^{5}	2	38.5	28	62	$H_2 + C_2H \leftrightarrow C_2H_2$ + H	4.09×10^{5}	2.4	3.6	28
22	CH + H_2 ⇔ H + CH_2	1.11×10^{8}	1.8	7.0	28	63	C_2H_3 + H ⇔ C_2H_2 + H_2	4.00×10^{13}	0	0.0	28
23	CH + CH_2 ⇔ H + C_2H_2	4.00×10^{13}	0	0.0	28	64	$C_2H + C_2H_2 \leftrightarrow C_4H_2$ + H	3.00×10^{13}	0	0.0	43
24	CH + CH_3 ⇔ H + C_2H_3	3.00×10^{13}	0	0.0	28	65	$C_2H_2 + C_2H_2 \leftrightarrow C_4H_3$ + H	9.40×10^{21}	−1.8	346.4	29
25	CH + CH_4 ⇔ H + C_2H_4	6.00×10^{13}	0	0.0	28	66	C_4H_3 + M ⇔ C_4H_2 + H + M	1.00×10^{16}	0	249.8	47
26	CH + CO (+M) ⇔ HCCO (+M)	5.00×10^{13}	0	0.0	28	67	C_2H_2 + M ⇔ C_2H + H + M	4.20×10^{16}	0	447.7	28
27	CH + HCCO ⇔ CO + C_2H_2	5.00×10^{13}	0	0.0	28	68	H + H + M ⇔ H_2 + M	1.00×10^{18}	−1	0.0	28
28	CH_2 + CO (+M) ⇔ CH_2CO (+M)	8.10×10^{11}	0.5	18.9	28	69	H + H + H_2 ⇔ H_2 + H_2	9.20×10^{16}	−0.6	0.0	28
29	H + CH_2 (+M) ⇔ CH_3 (+M)	2.50×10^{16}	−0.8	0.0	28	70	$C_2H_3 + CH_3 \leftrightarrow C_3H_6$	2.50×10^{13}	0	0.0	38
30	CH_2(S) + Ar ⇔ CH_2 + Ar	9.00×10^{12}	0	2.5	28	71	C_2H_6 + CH ⇔ C_3H_6 + H	1.10×10^{14}	0	−1.3	43
31	CH_2(S) + H_2 ⇔ CH_3 + H	7.00×10^{13}	0	0.0	28	72	C_3H_4P + M ⇔ C_3H_3 + H + M	3.50×10^{101}	−23.1	597.9	29
32	CH_2(S) + CH_3 ⇔ H + C_2H_4	1.20×10^{13}	0	−2.4	28	73	$CH_3 + C_3H_3 \leftrightarrow C_4H_6$	1.50×10^{12}	0	0.0	see text
33	CH_2(S) + CH_4 ⇔ $2CH_3$	1.60×10^{13}	0	−2.4	28	74	$CH_2 + C_3H_3 \leftrightarrow C_4H_4$ + H	3.00×10^{13}	0	0.0	est
34	CH_2(S) + CO ⇔ CH_2 + CO	9.00×10^{12}	0	0.0	28	75	$2C_3H_3 \leftrightarrow$ L−C_6H_6	6.00×10^{13}	0	0.0	est
35	CH_2(S) + C_2H_2 ⇔ C_3H_3 + H	1.80×10^{14}	0	0.0	36	76	L−C_6H_6 ⇔ C_6H_6	2.00×10^{12}	0	221.8	est
36	CH_2(S) + C_2H_4 ⇔ C_3H_6	9.60×10^{13}	0	0.0	36	77	C_6H_6 ⇔ C_6H_5 + H	2.00×10^{17}	0	494.1	48
37	H + CH_2CO ⇔ CH_3 + CO	1.10×10^{13}	0	14.4	42	78	C_6H_6 + H ⇔ $C_6H_5 + H_2$	6.00×10^{8}	1.8	68.4	49
38	H + CH_2CO ⇔ HCCO + H_2	5.00×10^{13}	0	33.5	28	79	$C_6H_6 + CH_3 \leftrightarrow C_6H_5 +$ CH_4	2.00×10^{12}	0	63.0	50
39	$CH_2 + H_2 \leftrightarrow$ H + CH_3	5.00×10^{5}	2	30.3	28	80	C_6H_5 ⇔ L−C_6H_5	4.00×10^{13}	0	305.1	43
40	$2CH_2$ ⇔ H + H + C_2H_2	1.00×10^{14}	0	0.0	43	81	L−C_6H_5 ⇔ $C_2H_2 + C_4H_3$	3.98×10^{62}	−14.7	240.6	51
41	$CH_2 + CH_3 \leftrightarrow$ H + C_2H_4	4.00×10^{13}	0	0.0	28	82	C_4H_6 ⇔ $C_4H_4 + H_2$	5.00×10^{14}	0	364.0	est

[a] ⇔ denotes reversible reaction. Reverse rate constant is calculated from the equilibrium constant. (+M) denotes a reaction in the falloff region; falloff parameters are given in the reference. furyl2: cyclic 2-furyl radical. furop1: formyl allene isomer structure **28**. furop2: formyl allene isomer structure **30**. C_3H_4P: propyne. [b] Units for A are $cm^3\ mol^{-1}\ s^{-1}$ or s^{-1} as appropriate. Units for E_a are kJ mol^{-1}. [c] PW denotes a rate constant determined in the present work, abin denotes a rate constant evaluated by ab initio calculation, and est denotes a rate constant estimated in the present work.

pathways for the disappearance of furan. Therefore, only these two major pathways are included in the kinetic model. The rate constant for the abstraction of hydrogen from furan by methyl was found to be $2.3 \times 10^{10}\ cm^3\ mol^{-1}\ s^{-1}$, and these pathways are also included in the kinetic model as a single pathway.

Considering now the fate of formyl allene (**28**), the forward and reverse rate constants for isomerization to its rotamer (**30**) at 1400 K were found to be 3.0×10^{12} and $1.5 \times 10^{12}\ s^{-1}$, respectively, while the rate constant for the decomposition of **30** to propyne and CO was computed to be $9.1 \times 10^{6}\ s^{-1}$. The rate constant associated with the decomposition of the formyl allenes (**28** and **30**) to propargyl and formyl radicals were found to be 2.4×10^{4} and $9.8 \times 10^{3}\ s^{-1}$, respectively. Thus, as expected from the energetics alone (see Figure 4), formyl allene is converted predominantly to propyne and CO. Propargyl and formyl are also products of the decomposition reaction of formyl propyne, but because rate constants for formation of these radicals from formyl propyne are significantly lower than from formyl allene, only the routes to HCO and C_3H_3 from the allene were considered in the kinetic model.

Kinetic Model. In the model, formulated on the basis of our ab initio results and summarized in Table 3, pyrolysis is initiated via 1,2-H migration from C(3) to C(2) and subsequent ring fissioning to the formyl allene (structure **28**) as shown in Figure 4. This is reaction 5 of the model, as shown in Table 3. This reaction was found to exhibit considerable sensitivity and therefore to optimize the computed furan and product profiles; the activation energy was reduced slightly from the ab initio value of 294.1 to 292.9 kJ mol^{-1}. In a parallel initiation, involving H migration from C(2) to C(3), furan can form ketene

and acetylene as shown in Figure 3. This is reaction 10 in Table 3. The Arrhenius parameters derived from the given potential energy surface, as described above, were 1.5×10^{15} s^{-1} and 344 kJ mol^{-1}. Reaction 10 is a very sensitive reaction for formation of acetylene, and in the course of modeling it was found that a reduction of the *A* factor to 9.0×10^{14} s^{-1}, while maintaining the ab initio value of the activation energy, improved the agreement between the computed and experimental acetylene profiles. We consider that such a difference between the model and ab initio values of A_{10} are within the expected uncertainty in the theoretical calculations. The rate constant for isomerization of the formyl allenes (reaction 6) was taken directly from the ab initio calculations as were rate constants for reactions 7−9, fission of the two formyl allenes into HCO and C_3H_3 and of formyl allene (structure **30**) into CO and propyne. *Not* included in the model is the direct ring-opening reaction of furan. Ring scission to form products on a singlet surface is clearly far too energetic a process. Ring opening with formation of CO + vinylmethylene on a triplet surface is computed from the ab initio results (based on the G2(MP2) estimate of treating **8** as the transition state) to have a rate constant of 1.8×10^{15} exp[−359 kJ mol^{-1}/(*RT*)] s^{-1}. This process is far to slow to contribute in any significant way to the rate of decomposition of furan. Even if the activation energy were reduced by 20 kJ mol^{-1}, which is judged to be about the maximum possible error in the ab initio calculations, the rate of decomposition of furan would not increase to an appreciable extent, as found by such experiments with the model. We are therefore forced to the conclusion that earlier mechanistic postulates that relied on ring fission to initiate pyrolysis are likely to be incorrect.

The model also contains secondary reactions of the principal products. Many of these reactions are included in the GRIMech2 mechanism,[28] and rate constants have been taken principally from this source. Because the primary product ketene decomposes largely into methylene radicals, reactions of both triplet methylene, CH_2, and of the singlet, $CH_2(S)$, have been included in the model with rate constants taken from GRIMech2 and other sources. Reactions of CH are also included, although these are not sensitive reactions.

During the initial phases of its development, this model gave good agreement between the modeled and experimental profiles for most major species, the exceptions being methane and ethylene, the former product being modeled at less than a tenth of the experimental yields. Methane arises from abstraction reactions of methyl radicals whose principal source is propyne via the addition of H and elimination of CH_3 (reaction 45) whose rate constant was taken from the NIST database.[29] Initially, methyl abstraction reactions with furan were not included in the model because we thought that on account of the strong CH bonds in furan such reactions would be unimportant. However, modeling revealed that there are insufficient sources of abstractable hydrogen in the products propyne, ketene, hydrogen, and acetylene to account for the observed yields of methane. Thus, despite the high barrier for abstraction, it was necessary to include an abstraction reaction between CH_3 and furan (reaction 2) in order to model the observed methane and ethylene satisfactorily. There are, in fact, two distinct types of abstractable hydrogens in furan, viz., those on C(2) and C(3), resulting in the two ring radicals 2-furyl and 3-furyl. Rate constants for both reactions were obtained via quantum chemical calculations, as described in an earlier section. For simplicity, we have only included abstraction to form 2-furyl + CH_4 because the abstraction to form the 3-furyl radical would ultimately lead to similar products. To optimize the predicted methane profiles by the kinetic model, we found it necessary to reduce the ab initio calculated activation energy for formation of 2-furyl of 96.9 kJ mol^{-1} by 9 kJ mol^{-1}. This reduction in activation energy is within the bounds of the uncertainty in the ab initio calculations. The 2-furyl radicals would be expected on thermochemical grounds to scission into CO and C_3H_3 (reaction 4), and because it is not a sensitive reaction, we empirically estimated its rate constant. Other abstraction reactions involving furan are reactions 1 (abstraction by CH_2) and 3 (abstraction by H). Neither is a sensitive reaction, and rate constants for these have been also estimated.

Kinetic modeling using the reaction model given in Table 3 was carried out using the Sandia CHEMKIN code[30] together with the shock tube code[31] (modified to allow for cooling by the reflected rarefaction wave) and the ordinary differential equation solver LSODE.[32] The predicted furan and product profiles are compared with experimental results[5] in Figure 7. Rate sensitivity analysis was carried out on the model using the SENKIN code.[33] Reverse rate constants have been evaluated using the equilibrium constants that were calculated from the thermochemistry by standard methods.

The results of sensitivity analysis of the kinetic model are shown in Table 4. The most sensitive reaction for decomposition of furan and for formation of most major products is reaction 5, the 1,2-H migration leading to the formation of the intermediate formyl allene, the precursor of propyne and CO. Also exhibiting considerable sensitivity is reaction 10, the hydrogen migration reaction leading to production of ketene and acetylene. Indeed, reaction 10 is the most sensitive reaction for formation of these two products. Other reactions exhibiting significant sensitivity are reaction 2, the methyl abstraction reaction with furan, reaction 45, the H addition to propyne and methyl displacement reaction, and reaction 72, fission of H from propyne. Ethylene profiles were sensitive for reaction 44, addition of CH_3 to ketene with fission into ethyl radicals + CO. The only previous estimate of the rate constant for this reaction is by Woods and Haynes.[34] However, their value of 5×10^{12} cm^3 mol^{-1} s^{-1} led to gross overestimates in the ethylene profiles. We find that a value of 4×10^{11} cm^3 mol^{-1} s^{-1} gives much better agreement with experimental results.

Small yields of 1,3-butadiene were observed in the earlier experimental work. In our model C_4H_6 principally arises via reaction 73, recombination of CH_3 and C_3H_3 radicals. Wu and Kern[35] previously estimated the rate constant of this reaction to be 5×10^{12} cm^3 mol^{-1} s^{-1}. We have reduced this rate constant to 1.5×10^{12} to obtain better agreement with experimental C_4H_6 profiles.

The kinetic model gives acceptable agreement with experimental furan profiles at the three concentrations studied experimentally, viz., 2.0, 1.0, and 0.2 mol % furan in Ar. Good agreement is also obtained for all major products except for ketene. It should be noted that the original experimental ketene profiles were subject to a considerable degree of experimental artifact. They were obtained by FTIR difference spectrometry with long acquisition times during which there was considerable loss of ketene due to subsequent reaction and/or adsorption in the spectrometer cell. Consequently, the ketene profiles produced by the model, which are a factor of 2−3 larger than those recorded by Organ and Mackie,[5] could well be quite reasonable.

The present kinetic model for furan pyrolysis, based on the ab initio calculations, differs significantly from that presented previously. As pointed out in the Introduction, previous experiments suggested a rate constant of $k_\infty = 10^{15.3\pm0.4}$ exp[−325 ±

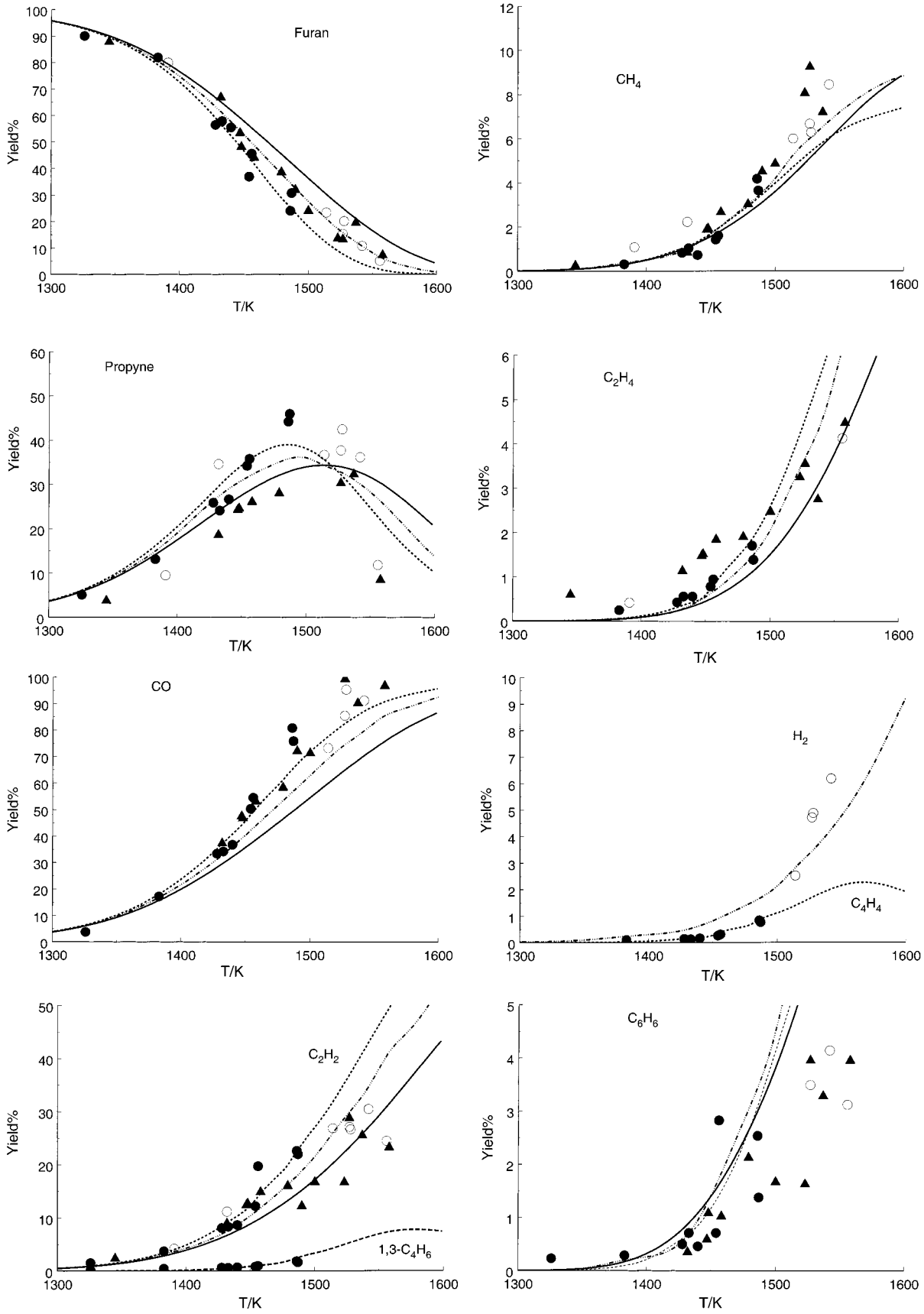

Figure 7. Temperature dependence of designated species in the pyrolysis of furan: (▲) data points at initial furan concentration of 2.0 mol %; (○) data points at initial furan concentration of 1.0 mol %; (●) data points at initial furan concentration of 0.2 mol % (all three sets from ref 5); (—) model prediction for 2.0%; (—···) model prediction for 1.0%; (- - -) model prediction for 0.2%.

10 kJ mol^{-1}/(RT)] s^{-1} for disappearance of furan, although the assumption that this rate constant may be equated with ring fission to a biradical would no longer appear to be tenable. Does the present model support the experimental rate parameters for

TABLE 4: Mole Fraction Sensitivity Coefficients [$\partial \log(\text{Yield}_i)/\partial \log k_j$] at 1533 K and 50 μs for Key Species in the Pyrolysis of Furan

reaction no.[a]	furan	CO	C_2H_2	C_3H_4P	CH_2CO	CH_4	C_2H_4	C_6H_6	H_2
2	−0.005	0.009	−0.010	0.005		0.384	−0.324	0.165	
3	−0.003		−0.033	0.007	0.010	−0.162	−0.176	0.196	0.440
5	−0.324	0.715	−0.023	0.737	−0.276	0.723	0.492	1.08	0.119
9	−0.003	0.007		0.013					−0.043
10	−0.076	−0.063	0.712	−0.078	0.921	−0.124	0.735	−0.151	0.109
37		0.007	−0.009		−0.026				−0.050
38					−0.021				0.162
44			0.008		−0.026		0.760		
45			0.095	−0.058	0.014	0.344	0.313	0.141	−0.391
47				−0.007		0.156			
72	−0.003	0.014	0.056	−0.079	−0.036	0.249	0.279	0.716	0.438
73								−0.091	
76								0.931	

[a] Reaction number as given in Table 3.

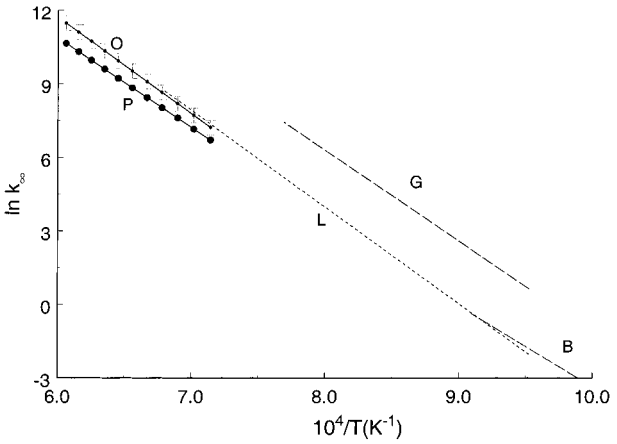

Figure 8. Arrhenius plots of the rate constants for disappearance of furan: (P) present model prediction; (O) Organ and Mackie (ref 5) with maximum errors in data; (L) Lifshitz et al. (ref 4); (G) Grela et al. (ref 3); (B) Bruinsma et al. (ref 6).

disappearance of furan? Organ and Mackie[5] made their measurements of this rate constant from time-resolved laser absorption profiles of furan over the temperature range 1464−1632 K. Experimentally, the disappearance of furan exhibited first-order kinetics to a good degree of approximation over a 10-fold range of furan concentration. Assuming first-order behavior, a plot of $\ln\{-(1/t')\ln(\text{furan}_{t'}/\text{furan}_{t=0})\}$ versus $1/T$ for small $t' = 10$ μs, when secondary processes should be negligible, enables apparent Arrhenius parameters for disappearance of furan to be obtained from the model. As may be seen in Figure 8, the model predicts Arrhenius behavior between 1400 and 1650 K with the parameters $A = 2 \times 10^{14}$ s^{-1} and $E_a = 303$ kJ mol^{-1}. Also shown in Figure 8 are data for the temperature dependence of the rate constant, as measured by previous workers, including error estimates, as published by Organ and Mackie.

As may be seen from Figure 8, the kinetic model predicts high-temperature rate constants that are lower than experimental values, although just outside the error limits of Organ and Mackie. When extrapolated to lower temperatures, the agreement with previous measurements is quite good.

The kinetic model supports the mechanism of two parallel furan decomposition routes to the major products CO + propyne and acetylene + ketene. No significant channel to C_3H_3 + HCO has been detected. Reactions 7 and 8 in which the intermediate formyl allenes fission into C_3H_3 + HCO have barriers that are too large to enable sufficient reaction flux to flow to these radical products. Organ and Mackie originally proposed such a route to account for H formation and also for the formation of benzene via C_3H_3 recombination. Analysis of the present model suggests that propyne is the principal source of both H and C_3H_3. Overwhelmingly, the major flux forming these two radicals arises from CH fission of propyne (reaction 72).

Conclusions

The current ab initio calculations suggest that the barrier to direct ring scission, either on a singlet or triplet surface, is much too high and therefore the associated rate of decomposition is much too slow to account for the experimentally observed kinetics of furan pyrolysis. On the other hand two parallel processes, one proceeding via a H-transfer from C(3) to C(2) in furan and the other involving a H-transfer from C(2) to C(3), which result in the formation of cyclic carbene intermediates, enable the kinetics of furan disappearance and the formation of the major products, viz., CO, propyne, acetylene, and ketene, to be satisfactorily modeled. The first of these two parallel channels is the major one, leading to the products CO + propyne; the minor channel produces C_2H_2 + ketene. No evidence was found for significant participation of a third channel that might produce HCO + C_3H_3. H atoms and C_3H_3 radicals instead arise essentially from CH fission of propyne. Methane in the products was found to arise principally by abstraction of a CH bond in furan even though the bond enthalpies are 506 and 514 kJ mol^{-1} for the two distinct bonds. A kinetic model containing rate constants derived from the ab initio calculations can satisfactorily model the species profiles that had been obtained in shock tube experiments at three initial concentrations of furan.

Acknowledgment. K.S. gratefully acknowledges the award of an Australian Postgraduate Research Scholarship.

Supporting Information Available: Tables S1−S4 listing optimized geometries, energies, rotational constants, and vibrational frequencies. This material is available free of charge via the Internet at http://pubs.acs.org.

References and Notes

(1) Lee, J. H.; Tang, I. N. *J. Chem. Phys.* **1982**, *77*, 4459.
(2) Fulle, D.; Dib, A.; Kiefer, J. H.; Zhang, Q.; Yao, J.; Kern, R. D. *J. Phys. Chem. A* **1998**, *102*, 7480.
(3) Grela, M. A.; Amorebieta, V. T.; Colussi, A. J. *J. Phys. Chem.* **1985**, *89*, 38.
(4) Lifshitz, A.; Bidani, M.; Bidani, S. *J. Phys. Chem.* **1986**, *90*, 5373.
(5) Organ, P. P.; Mackie, J. C. *J. Chem. Soc., Faraday Trans.* **1991**, *87*, 815.
(6) Bruinsma, O. S. L.; Tromp, P. J. J.; de Sauvage Nolting, H. J. J.; Moulijn, J. A. *Fuel* **1988**, *67*, 334.

(7) Benson, S. W. *Thermochemical Kinetics*, 2nd ed.; Wiley: New York, 1976.
(8) Bacskay, G. B.; Martoprawiro, M.; Mackie, J. C. *Chem. Phys. Lett.* **1999**, *300*, 321.
(9) Martoprawiro, M.; Bacskay, G. B.; Mackie, J. C. *J. Phys. Chem. A* **1999**, *103*, 3923.
(10) Wilsey, S.; Bearpark, M. J.; Bernardi, F.; Olivucci, M.; Robb, M. A. *J. Am. Chem. Soc.* **1996**, *118*, 4469.
(11) Liu, R.; Zhou, X.; Zhai, L. *J. Comput. Chem.* **1998**, *19*, 240.
(12) Litwinowicz, J. A.; Ewing, D. W.; Jurisevic, S.; Manka, M. J. *J. Phys. Chem.* **1995**, *99*, 9709.
(13) Roos, B. O.; Taylor, P. R.; Siegbahn, P. E. S. *Chem. Phys.* **1980,** *48*, 157.
(14) Roos, B. O. In *Ab initio Methods in Quantum Chemistry*; Lawley, K. P., Ed.; Wiley: Chichester, U.K., 1987; Vol. II, p 399.
(15) Dunning, T. H. *J. Chem. Phys.* **1987**, *90*, 1007.
(16) Woon, D. E.; Dunning, T. H. *J. Chem. Phys.* **1990**, *98*, 1358.
(17) Andersson, K.; Malmqvist, P.-Å.; Roos, B. O.; Sadlej, A. J.; Wolinski, K. *J. Chem. Phys.* **1990**, *94*, 5483.
(18) Andersson, K.; Malmqvist, P.-Å.; Roos, B. O. *J. Chem. Phys.* **1992**, *96*, 1282.
(19) Curtiss, L. A.; Raghavachari, K.; Pople, J. A. *J. Chem. Phys.* **1993**, *98*, 1293.
(20) Andersson, K.; Roos, B. O. *Int. J. Quantum Chem.* **1993**, *45*, 591.
(21) Steinfeld, J. I.; Francisco, J. S.; Hase, W. L. *Chemical Kinetics and Dynamics*; Prentice Hall: Englewood Cliffs, NJ, 1989; p 308.
(22) McQuarrie, D. A. *Statistical Mechanics*; Harper & Row: New York, 1973; p 129.
(23) Hase, W. L.; Mondro, S. L.; Duchovic, R. J.; Hirst, D. M. *J. Am. Chem. Soc.* **1987**, *109*, 2916.
(24) DALTON, an ab initio electronic structure program, release 1.0, 1997, written by T. Helgaker, H. J. Aa. Jensen, P. Joergensen, J. Olsen, K. Ruud, H. Aagren, T. Andersen, K. L. Bak, V. Bakken, O. Christiansen, P. Dahle, E. K. Dalskov, T. Enevoldsen, B. Fernandez, H. Heiberg, H. Hettema, D. Jonsson, S. Kirpekar, R. Kobayashi, H. Koch, K. V. Mikkelsen, P. Norman, M. J. Packer, T. Saue, P. R. Taylor, and O. Vahtras.
(25) Andersson, K.; Blomberg, M. R. A.; Fülscher, M. P.; Karlström, G.; Lindh, R.; Malmqvist, P.-Å; Neogrády, P.; Olsen, J.; Roos, B. O.; Sadlej, A. J.; Schütz, M.; Seijo, L.; Serrano-Andrés, L.; Siegbahn, P. E. M.; Widmark, P.-O. *MOLCAS*, version 4; Lund University: Lund, Sweden, 1997.
(26) Frisch, M. J.; Trucks, G. W.; Schlegel, H. B.; Scuseria, G. E.; Robb, M. A.; Cheeseman, J. R.; Zakrzewski, V. G.; Montgomery, J. A., Jr.; Stratmann, R. E.; Burant, J. C.; Dapprich, S.; Millam, J. M.; Daniels, A. D.; Kudin, K. N.; Strain, M. C.; Farkas, O.; Tomasi, J.; Barone, V.; Cossi, M.; Cammi, R.; Mennucci, B.; Pomelli, C.; Adamo, C.; Clifford, S.; Ochterski, J.; Petersson, G. A.; Ayala, P. Y.; Cui, Q.; Morokuma, K.; Malick, D. K.; Rabuck, A. D.; Raghavachari, K.; Foresman, J. B.; Cioslowski, J.; Ortiz, J. V.; Stefanov, B. B.; Liu, G.; Liashenko, A.; Piskorz, P.; Komaromi, I.; Gomperts, R.; Martin, R. L.; Fox, D. J.; Keith, T.; Al-Laham, M. A.; Peng, C. Y.; Nanayakkara, A.; Gonzalez, C.; Challacombe, M.; Gill, P. M. W.; Johnson, B. G.; Chen, W.; Wong, M. W.; Andres, J. L.; Head-Gordon, M.; Replogle, E. S.; Pople, J. A. *Gaussian 98*, revision A.1; Gaussian, Inc.: Pittsburgh, PA, 1998.
(27) Yoshimine, M.; Pacansky, J.; Honjou, N. *J. Am. Chem. Soc.* **1989**, *111*, 2785.
(28) Bowman, C. T.; Hanson, R. K.; Davidson, D. F.; Gardiner, W. C.; Lissianski, V.; Smith, G. P.; Golden, D. M.; Frenklach, M.; Goldenberg, M. *GRIMech*; http://www.me.berkeley.edu/gri_mech.
(29) Mallard, W. G.; Westley, F.; Herron, J. T.; Hampson, R. G.; Frizzell, D. H. *NIST Chemical Kinetic Database*, version 2Q98; National Institute of Standards and Technology: Gaithersburg, MD, 1998.
(30) Kee, R. J.; Miller, J. A.; Jefferson, T. H. *CHEMKIN: A General Purpose, Problem Independent, Transportable FORTRAN Chemical Kinetics Code Package*; Sandia National Laboratories Report SAND80-003; Sandia National Laboratories: Albuquerque, NM, March 1980.
(31) Mitchell, R. E.; Kee, R. J. *A General Purpose Computer Code for Predicting Chemical Kinetic Behavior Behind Incident and Reflected Shocks*; Sandia National Laboratories Report SAND82-8205; Sandia National Laboratories: Albuquerque, NM, March 1982.
(32) Hindmarsh, A. C. LSODE and LSODI: Two New Initial Value Differential Equation Solvers. *ACM Signum Newsl.* **1980**, *15* (4).
(33) Lutz, A. E.; Kee, R. J.; Miller, J. A. *SENKIN: A FORTRAN Program Predicting Homogeneous Gas-Phase Chemical Kinetics with Sensitivity Analysis*. Sandia National Laboratories Report SAND87-8248; Sandia National Laboratories: Albuquerque, NM, February 1988.
(34) Woods, I. T.; Haynes, B. S. *Proceedings of the 25th International Symposium on Combustion*; The Combustion Institute: Pittsburgh, PA, 1994; p 909.
(35) Wu, C. H.; Kern, R. D. *J. Phys. Chem.* **1987**, *91*, 6291.
(36) Baulch, D. L.; Cobos, C. J.; Cox, R. A.; Frank, P.; Hayman, G.; Just, Th.; Kerr, J. A.; Murrells, T.; Pilling, M. J.; Troe, J.; Walker, R. W.; Warnatz, J. J. *Phys. Chem. Ref. Data* **1994**, *23*, 847.
(37) Hidaka, Y.; Taniguchi, T.; Tanaka, H.; Kamesawa, T.; Inami, K.; Kawano, H. *Combust. Flame* **1993**, *92*, 365.
(38) Tsang, W.; Hampson, R. F. *J. Phys. Chem. Ref. Data* **1986**, *15*, 1087.
(39) Baggott, J. E.; Frey, H. M.; Lightfoot, P. D.; Walsh, R. *J. Phys. Chem.* **1987**, *91*, 3386.
(40) Frank, P.; Bhaskaran, K. A.; Just, Th. *Proceedings of the 21st International Symposium on Combustion*; The Combustion Institute: Pittsburgh, PA, 1986; p 885.
(41) Homann, K. H.; Wellmann, Ch. *Ber. Bunsen-Ges. Phys. Chem.* **1983**, *87*, 609.
(42) Michael, J. V.; Nava, D. F.; Payne, W. A.; Stief, L. J. *J. Chem. Phys.* **1979**, *70*, 5222.
(43) Baulch, D. L.; Cobos, C. J.; Cox, R. A.; Esser, C.; Frank, P.; Just, Th.; Kerr, J. A.; Pilling, M. J.; Troe, J.; Walker, R. W.; Warnatz, J. *J. Phys. Chem. Ref. Data* **1992**, *21*, 411.
(44) Fahr, A.; Stein, S. E. *Proceedings of the 22nd International Symposium on Combustion*; The Combustion Institute: Pittsburgh, PA, 1988; p 1023.
(45) Kiefer, J. H.; Al-Alami, M. Z.; Budach, K. A. *J. Phys. Chem.* **1982**, *86*, 808.
(46) Kiefer, J. H.; Mitchell, K. I.; Kern, R. D.; Yong, J. N. *J. Phys. Chem.* **1988**, *92*, 677.
(47) Wu, C. H.; Singh, H. J.; Kern, R. D. *Int. J. Chem. Kinet.* **1987**, *19*, 975.
(48) Kiefer, J. H.; Mizerka, L. J.; Patel, M. R.; Wei, H.-C. *J. Phys. Chem.* **1985**, *89*, 2013.
(49) Mebel, A. M.; Lin, M. C.; Yu, T.; Morokuma, K. *J. Phys. Chem. A* **1997**, *101*, 3189.
(50) Zhang, H. X.; Ahonkhai, S. I.; Back, M. H. *Can. J. Chem.* **1989**, *67*, 1541.
(51) Braun-Unkhoff, M.; Frank, P.; Just, Th. *Proceedings of the 22nd International Symposium on Combustion*; The Combustion Institute: Pittsburgh, PA, 1988; p 1053.